Carbonated Mantle: Modelling the effect of carbonated melts on mantle melting and conductivity

Thesis submitted in accordance with the requirements of the University of Adelaide for an Honours Degree in Geophysics

Angus Keane

November 2014

THE UNIVERSITY of ADELAIDE

CARBONATED-SILICATE MELTS

MODELLING THEIR EFFECT ON MANTLE CONDUCTIVITY

ABSTRACT

The effect of carbonated melts are observed to have significant deepening of the solidus and high conductivity as a function of CO_2 concentration in the melt. In this study parameterising these two effects, and present a model that determines mantle melt fraction and bulk hydration from conductivity observations, using the melting models of McKenzie and Bickle (1988), Katz et al. (2003), and Hirschmann (2010). This model is applied to conductivity data of Key et al. (2013) and (Wannamaker et al. 2008) for the East Pacific Rise and the Basin and Range, Colorado, respectively. Our interpretations of melting and hydration, are in agreement with those posed by the Key et al. (2013) and Wannamaker et al. (2008).

KEYWORDS : CARBONATED MELT, CARBONATE CONDUCTIVITY, CARBONATE SOLIDUS DEPRESSION

TABLE OF CONTENTS

LIST OF FIGURES AND TABLES

INTRODUCTION

Bulk mantle conductivity is a property influenced by bulk composition, melt fraction, and the physical environment at depth. By improving on models that relate bulk conductivity to these factors, we can more accurately infer the properties of the mantle at depth by utilising deep conductivity studies such as magnetotellurics.

It is widely accepted that mantle composition, pressure, temperature, hydration, as well as melt fraction and geometry, are factors which have a significant contribution to the conductivity response of the mantle (e.g.(Xu et al. 2000, Wang et al. 2008, Poe et al. 2010).

By making assumptions about mantle composition, fertility, and temperature and pressure regimes using global analogues, allows interpretations to be made about other variables such as hydration, and melt fraction which are much more variable. This is common practice in previous studies (Constable and Heinson 2004, Ledo and Jones 2005), which assume the composition of the mantle solid phase to be fertile or depleted peridotite, and of melt phases to be basaltic; as significant research and parameterisations have been done on both. (Constable 2006, Tyburczy and Waff 1983, Ni et al. 2011, etc.)

However in regions such as the East Pacific Rise, the conductivity values measured are only possible with an estimated 10% partial melting using interpretations from these assumptions (Key et al. 2013)This is in large disagreement with seismic observations of only 1-3% melt in the East Pacific Rise (Toomey et al. 1998, Hammond and Toomey 2003), indicating that these conventional assumptions are not always sufficient.

Close to the solidus, the melt is more carbonitic than silicate (<10% SiO2 and 38-45% CO_2 in melt, Dasgupta et al. (2013)) and as carbonitic melts are far more conductive than silicate melts, bulk conductivity for low melt fractions can increase drastically. Many studies have considered this, and suggested that anomalous conductivity in the EPR is a likely case, explainable with small volumes of carbonitic melt (e.g. (Kelbert et al. 2009, Hirschmann 2010) etc). Hence recently there has been more focus on parameterising the effects that variable concentrations of CO_2 in melt has on the mantle properties.

Although assuming a basaltic composition of melt may be sufficient for interpretations in mid oceanic ridges and regions of high melt production; for systems of low melt fraction and significant bulk CO_2 the interpretation of melt fraction from bulk conductivity may be overestimated as seen with the East Pacific Rise. This is owing to the oversight of a melt composition that is higher in conductivity than a basaltic melt. Yoshino et al. (2010) and Yoshino et al. (2012a) observed the effect of bulk CO_2 on peridotite compositions under high pressures, and found an effective increase in melt conductivity with increasing CO_2 concentration.

Conversely, assuming a basaltic melt composition where bulk CO_2 is present has been found to underestimate the melt fractions possible at depth. Dasgupta and Hirschmann (2006), WnNoreNDT and Myspx (1980), Hirose (1997, etc.)observed that carbonated partial melts are stabilised at greater depths than silicate partial melts due to a significant deepening effect on the solidus. This oversight results in underestimation of both the stability of larger melt fractions where CO_2 is present, and the depth to onset of partial melting.

In this study we parameterise carbonated melt conductivity and solidus depression, taking special interest on the experiments of Yoshino et al. (2012) and Dasgupta et al. (2013) who have observed the effect CO_2 concentration in melt has on melt conductivity and the solidus temperature respectively. Both studies made an attempt at parameterising these effects, however they did not model their results to be applied to variable conditions.

We then extrapolate their results to higher degrees of pressure and temperature and finally combine our results with previous work on modelling mantle properties from conductivity. Doing these, produce a more comprehensive method that includes effects of bulk CO_2.

Using our model, we then compare our results to two geophysical studies for interpretation of the mantle properties: hydration and melt fraction. These two studies are:

- The East Pacific Rise; a region of high conductivity but low estimated melt fraction. It is of interest to us as it is commonly suggested that the anomalous conductivity is a result of small volumes of carbonated melt. We seek to determine if for the conductivity ranges observed by Key et al. (2013), our model is sufficient to estimate melt fractions in agreement seismic estimates
- The Great Basin and Range; a region of particular interest as the presence of melt is indicative of the mode of the Colorado Great Basin/Colorado Plateau transition zone extension, whether it be pure shear (indicated by no melting), or simple shear along detachments (indicated by crustal underplating). There is also an availability of numerous petrologic, magnetotelluric, and seismic studies that have been conducted on this region for comparison with our

results (e.g.Selverstone et al. (1999), Smith and Griffin 2005). We aim to determine whether the conductivity ranges observed by Wannamaker et al. (2008), are possible with no melting when effects of bulk CO_2 are considered, and if the bulk hydration required is within a reasonable estimate.

BACKGROUND

Effect of carbonated-silicate melt

SOLIDUS DEPRESSION

Although it is well understood that CO_2 in melt depresses the solidus (Dasgupta and Hirschmann 2006, WnNoreNDT and Myspx 1980, Hirose 1997, etc.), the lack of data for these studies available at multiple pressures and variable concentrations of carbonated peridotite has not made a robust parameterization possible.

A study by Dasgupta et al. (2013) preformed melting experiments on compositions equivalent to fertile mantle peridotite, with 1.0% and 2.5% bulk CO_2 concentration. Their experiments were conducted over a range of 2–5 GPa and 1,300–1,750 °C to simulate Earth's oceanic upper-mantle conditions. However the aim of this paper was not to parameterize peridotite solidus depression by effect of CO_2, but to observe the magnitude of the depression effect at conditions similar to oceanic upper mantle. As a result this addressed the disagreement between geophysical observations of significant melt fraction at depth beneath mid oceanic ridges, and previous estimates of carbonate-silicate melting at the same depth (e.g. Dasgupta et al. (2007b)). Hence the model produced to fit the data was not a singular direct function of pressure and CO_2 concentration as required by this study, but rather a different model for each of the four

pressures as a function of CO_2 concentration. Due to the <25% CO_2 limit of most of the dataset, and the models chosen, there is also the restriction of Dasgupta's model being defined only for CO_2 <=25%, and pressures of 2-5 GPa, beyond which is purely an educated speculation on their behalf.

Whilst 2-5 GPa, and <25% X was sufficient for the field of interest of (Dasgupta et al. 2013), this model is not applicable outside of this range, and we require a new model that fits their data and is a direct function of CO_2 concentration and pressure.

CARBONATED PERIDOTITE MELT CONDUCTIVITY

There have be a number of observations of the conductivity of carbonated silicate (see (Gaillard et al. 2008, Yoshino et al. 2010)however there has been little attempt in these studies to extrapolate results to form a continuous relationship.

Yoshino (2012) observed a good linear relationship in an Arrhenius plot (logσ vs. 1/T) in five peridotite samples of varying CO_2 concentration, at temperatures above 1400K, and applied the below Arrhenius relationship:

$$\sigma_{bulk} = \sigma_{0,bulk} \exp\left(-\frac{dH}{RT}\right)$$

$$\mathrm{Log}_{10}(\sigma_{bulk}) = \mathrm{Log}_{10}\sigma_{0,bulk} - \left(\frac{dH}{RT}\right)\mathrm{Log}_{10}(\exp(1))$$

Each samples activation enthalpy (dH) and Logarithmic pre-exponential factor(σ_0) were assumed to hold a linear relationship between the fixed activation enthalpies of pure carbonate and pure silicate melt as a function of X. Using this assumption, and the relationship known as Archie's law, Yoshino et al. (2012a) was able to calculate activation enthalpy (dH) and Logarithmic pre-exponential factor (σ_0) by utilizing

information from the samples volume melt fraction (φ), sampling temperature (T_{samp}), and CO_2 concentration by wt.%, where $Log\sigma 0_{150}$ refers to assuming activation enthalpy for that of basaltic melt (150 kJ/mol):

$$dH_{melt} = dH_{dol} + (dH_{bas} - dH_{dol}) * \left(1 - \frac{X_{co2}}{50}\right)$$

$$Log\sigma 0_{38} = Log\sigma_{bulk} - \left(-\frac{38}{RT_{samp}}\right) * Log(e^1) + Log(C\varphi^n)$$

$$Log\sigma 0_{150} = Log\sigma_{bulk} - \left(-\frac{150}{RT_{samp}}\right) * Log(e^1) + Log(C\varphi^n)$$

$$Log\sigma_{0,melt} = Log\sigma 0_{38} + (Log\sigma 0_{150} - Log\sigma 0_{38}) * \left(1 - \frac{X_{co2}}{50}\right)$$

However the constants used in calculating Archie's law: C and n, are specific to the sample composition, and were not linearly related. Therefore a direct relationship between σ_{melt} and X_{CO2} was not produced.

Mantle Melting

Parameterisations of peridotite melting have made increasing developments in parallel with the advancement of analytical techniques since the empirical melting model of McKenzie and Bickle (1988). In this paper we present three different bulk melt parameterisations for use, on the basis that each model considers different compositional and physical effects:

- McKenzie and Bickle (1988) developed an empirical model for parameterising peridotite decompression-melt production as a function of

temperature and pressure. The model we use has extended to a hydrous extension case by Davies and Bickle (1991).

- Katz et al. (2003) developed a model in which melting is a function of pressure, temperature, and bulk H_20, considering the effect of modal CPX melting on melt production.
- Hirschmann (2010)

The effect solidus depression by effect of carbonated melt is accumulative with the depression effect of H_2O concentration in bulk melt, and takes the form described by Katz et al. (2003):

$$T_{solidus}^{H_2O,CO_2} = T_{sol}^{vf} - (\Delta T^{H_2O} + \Delta T^{CO_2})$$

$$T_{liquidus}^{H_2O,CO_2} = T_{liq}^{vf} - (\Delta T^{H_2O} + \Delta T^{CO_2})$$

where T^{vf} refers to the volatile free solidus.

Mantle conductivity

The bulk conductivity depends on the conductivity of individual phases, the total volume melt fraction, and the melt geometry. The Hashin-Shtrikman bounds are widely recognized to be accurate and upper bounds on conductivity in the absence of knowledge of the geometrical arrangement of N phases:

$$\mathrm{HS}^- = \left(\sum_{i=1}^{N} \frac{\phi_i}{\sigma_i + 2\sigma_{min}}\right)^{-1} - 2\sigma_{min} \qquad \mathrm{HS}^+ = \left(\sum_{i=1}^{N} \frac{\phi_i}{\sigma_i + 2\sigma_{max}}\right)^{-1} - 2\sigma_{max}$$

Where $\sigma_{max}/\sigma_{min}$ refers to the largest and smallest conductivity of the N phases, and ϕ_i and σ_i refers to the volume fraction and conductivity of phase (i) (Carcione et al. 2007). The Hashin-Shtrikman model assumes the best case and worst case scenario for

melt geometry. It does so by assuming isolated resistive spheres in interconnected conductive matrix (upper bound) or isolated conductive spheres in a resistive matrix (lower bound) (Hashin and Shtrikman 1963).

In most of the upper mantle, partial melting of peridotite behaves as a miscible mix of silicate and carbonate melt (Dasgupta and Hirschmann 2010, Dasgupta et al. 2007a), whereas an immiscible mix of carbonated and silicate melt phases is more commonly found shallow melting of carbonated mafic eclogite. (Dasgupta and Hirschmann 2010), and as such there are therefore two possible choices of phases relationships in the HS bounds:

- Solid phase, with a miscible carbonate silicate melt phase; or
- Solid phase, with an immiscible carbonated melt phase, and an immiscible silicate melt phase.

Although we acknowledge the likelihood of the former, the immiscible melt case was chosen to extend to HS bounds to both cases. This is because a system of interconnected carbonitic melt in a silicate and solid matrix is more conductive than a system of interconnected miscible melt, representing a true upper bound in absence of knowledge of melt geometry. The partitioning of bulk melt between immiscible silicate and carbonated melt is taken as a function of CO_2 concentration in melt (Hasterok 2014) (Figure 1).

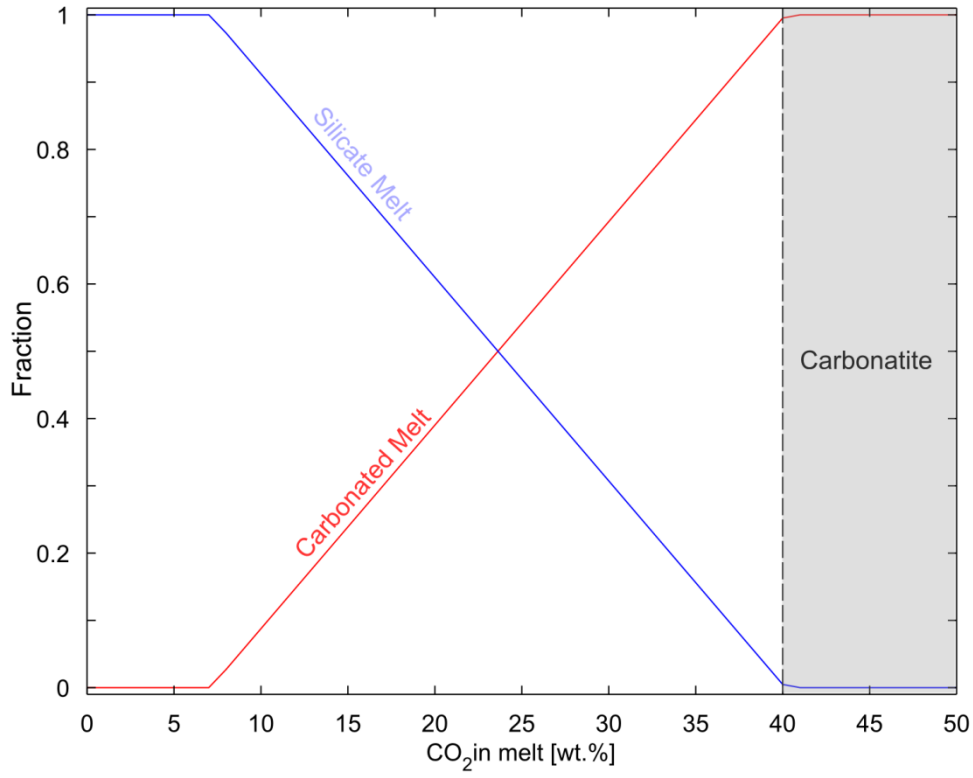

Figure 1:Partitioning of bulk melt fraction between immiscible silicate and carbonated melt taken from Hasterok (2014). Vertical axis is the respective fraction.

Typically, olivine only constitutes about 60-70% of fertile mantle peridotite; the other 40-30% consisting of major phases orthopyroxene and clinopyroxene; and other minor phases of <5% such as spinel (Simpson and Bahr 2005, Green and Ringwood 1963, Simpson 2002, etc.). Although there are a number of studies on the conductivity of the pyroxenes (e.g. Yang et al. (2011), Dai and Karato (2009)), the problem lies in that there has not been as comprehensive work in parameterising conductivity, and water partitioning between the pyroxenes and the other phases as a function of pressure, as there has been with olivine. It is justified to assume that the conductivity of the solid phase can be calculated with the conductivity of olivine as there is near negligible variation of bulk conductivity between fertile peridotite, and Dunite (>90% olivine)

(Dvorak 1973), and in presence of melt is almost entirely negligible (Roberts and Tyburczy 1999).

There are numerous experimental studies on basalts that quantify the conductivity of silicate melts using the Arrhenius relationship, however this is not a standard model for silicate melt as the conductivity is strongly dependant on hydration, composition and pressure, which are not considered in the Arrhenius relationship. Originally this study intended to use the "SigMelts" method of Pommier (2012) which computes silicate melt conductivity as a function of pressure, temperature, and melt composition to determine conductivity, however this method is limited to 2GPa, and would not be applicable to a comprehensive model. Therefore due to its agreement with the 0 wt% CO_2 values of Yoshino et al. (2012a), the silicate melt phase conductivity used in this study is taken from Pommier et al. (2010) results on Kilauea basalt.

Its noted here that the tradeoff for a silicate melt model that is applicable to high pressure and temperature, is an underestimation conductivity by effect of water content. It is well known that the addition of water reduces the activation enthalpy of melt thereby reducing the conductivity dependence of temperature on the system and is likely to reflect the effect of water incorporation increasing sodium ionic mobility in melts (Gaillard 2004). By using the fixed enthalpy of (Pommier et al. 2010), the conductivity of the melt is unaffected by water partitioning between the solid phase into the melt. It would be of interest of future studies to parameterise the change in activation enthalpy, possibly with a method similarly used on olivine in (Yoshino et al. 2009)

METHODS

Modeling Effects of CO_2

SOLIDUS DEPRESSION BY EFFECT OF CO_2 CONCENTRATION

Experimental results of Dasgupta et al. (2007a) and (Dasgupta et al. 2013), are plotted on a DT vs. CO_2 melt concentration plot using the volatile-free solidus temperatures from Hirschmann (2000), as done in both papers.

Considering other similar starting models with variable parameters, the data was fit using the inverse Newton method by a model of the form:

$$\Delta T_{CO2} = a_1 X + a_2 P \tan^{-1}(a_3 X)$$

Data that did not have melting or known error in CO_2 concentration are excluded from fitting as it would poorly bias the results. This form was chosen largely due to its simplicity, its application to very low pressure, how well it fit the data at 40-45% CO_2, and its saturation for large values of

An accurate model between 25-50% CO_2 is crucial to very small melt fractions, which is why the quality of fit here is a critical consideration to this model. However with more data, we may find that one of the other starting models considered would be a far more competent fit.

MODELLING CARBONATED SILICATE CONDUCTIVITY BY EFFECT OF CO_2 CONCENTRATION

Using the results of Yoshino et al. (2012b) samples; in attempt to determine a model for the pre exponential factor as a function of CO_2, the determined $Log_{10}\sigma_0$ were plotted against CO_2 concentration in melt (Figure 2), and was observed to hold linear relationship of the form:

$$Log_{10}\sigma_0 = b_1 X + b_2$$

The model produced for logs0, and the linear relationship of dH described in Yoshino 2012 are then returned to the Arrhenius relationship to give an equation of the form:

$$\log \sigma_m = (b_1 X + b_2) - \left(\frac{38 + (150 - 38)(1 - \frac{X}{50})}{RT * \log(10)} \right)$$

$$\sigma_{melt} = 10^{(b_1 X + b_2)} \exp\left(-\left(\frac{150 - 56\left(\frac{X}{25}\right)}{RT} \right) \right)$$

This model is significantly different from the fitting produced in Yoshino 2012, however has far more mathematical basis to the parameterization (see appendix for further derivation).

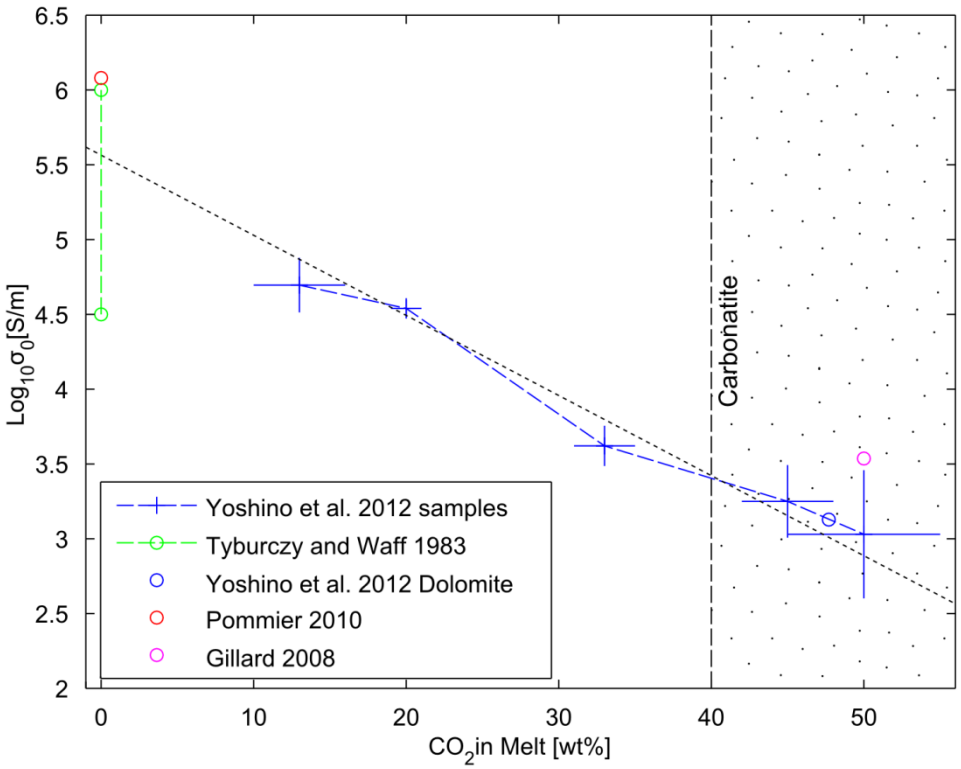

Figure 2:Plot of sample melt pre exponential factor σ_0 against sample CO_2 concentration. Results of Tyburczy and Waff (1983), dolomite sample of Yoshino et al. (2012a), Pommier et al. (2010), and Gaillard et al. (2008) are plot for comparison

Modeling the Mantle Properties

We estimate the physical properties of the mantle from observed conductivity by modeling the range of possible bulk conductivities at depth. However due to the number of variables that have significant control over bulk conductivity, we make the following assumptions to simplify the system:

1. The Bulk mineral assemblage, and chemical composition are assumed.
   This can be done quantitatively from xenolithic evidence, or qualitative assumptions of the mantle through global analogues (e.g. a mid ocean ridge would imply depleted peridotite, a hotspot would imply fertile peridotite)
   Again, in this study we assume the solid phase is constituted of olivine only.

2. Lateral variations in mantle pressure and temperature are negligible
   With this assertion, it can be assumed that mantle pressure and temperature are a direct function of depth. This study uses a depth profile that accounts for Moho depth, crustal and mantle densities, and follows mantle adiabatic temperature.

In making these assumptions, the conductivity range possible for a given depth, can then be modeled as a function of melt fraction and some unknown variable property. As we seek to apply this model to inferring the range of bulk hydration of the mantle, bulk hydration is chosen as this variable parameter.

The calculation scheme for conductivity as a function of depth and hydration is then as follows:

1. Estimate multiple bulk Melt fractions over a range of depths and bulk hydrations, considering the initial assumptions and using one of the prior melting models
2. Determine the partitioning of the bulk melt fraction between immiscible carbonated and silicate melts based on the carbonated melt-silicate melt mixing model (Hasterok 2014)
3. Determine partitioning of bulk chemistry to each phase
4. Reject melt fraction estimates based on chemical limitations of solubility. In this study rejections are made when H2O in the solid phase exceeds the saturation of olivine, taken from Hirschmann et al. (2005).
5. Calculate the conductivity of each phase using the conductivity models prior described
6. Estimate the upper and lower bounds of bulk conductivity using the HS bounds

Doing the method above produces a range of conductivities possible as a function of bulk water content at a given depth and composition. As the HS lower conductivity bounds are usually quite extensive, it requires some human intervention here to determine ranges based on plausibility or well these values agree with other studies.

OBSERVATIONS AND RESULTS

Solidus Depression model

The experimental dataset of Dasgupta et al. (2007b) and Dasgupta et al. (2013) for pressure 2-5 GPa was fit by the model:

$$\Delta T_{CO2} = a_1 X + a_2 P \tan^{-1}(a_3 X)$$

Where a_1 = 0.57, a_2 = -47.87, and a_3 = 0.06. This model of solidus depression by effect of carbonated melt is combined accumulatively with the solidus depression by effect of water concentration in melt. The resulting adjustment to the volatile free solidus for melt models of McKenzie and Bickle (1988), Hirschmann (2010) and Katz et al. (2003) have been plotted for comparison at varying bulk compositions (Figure 3)

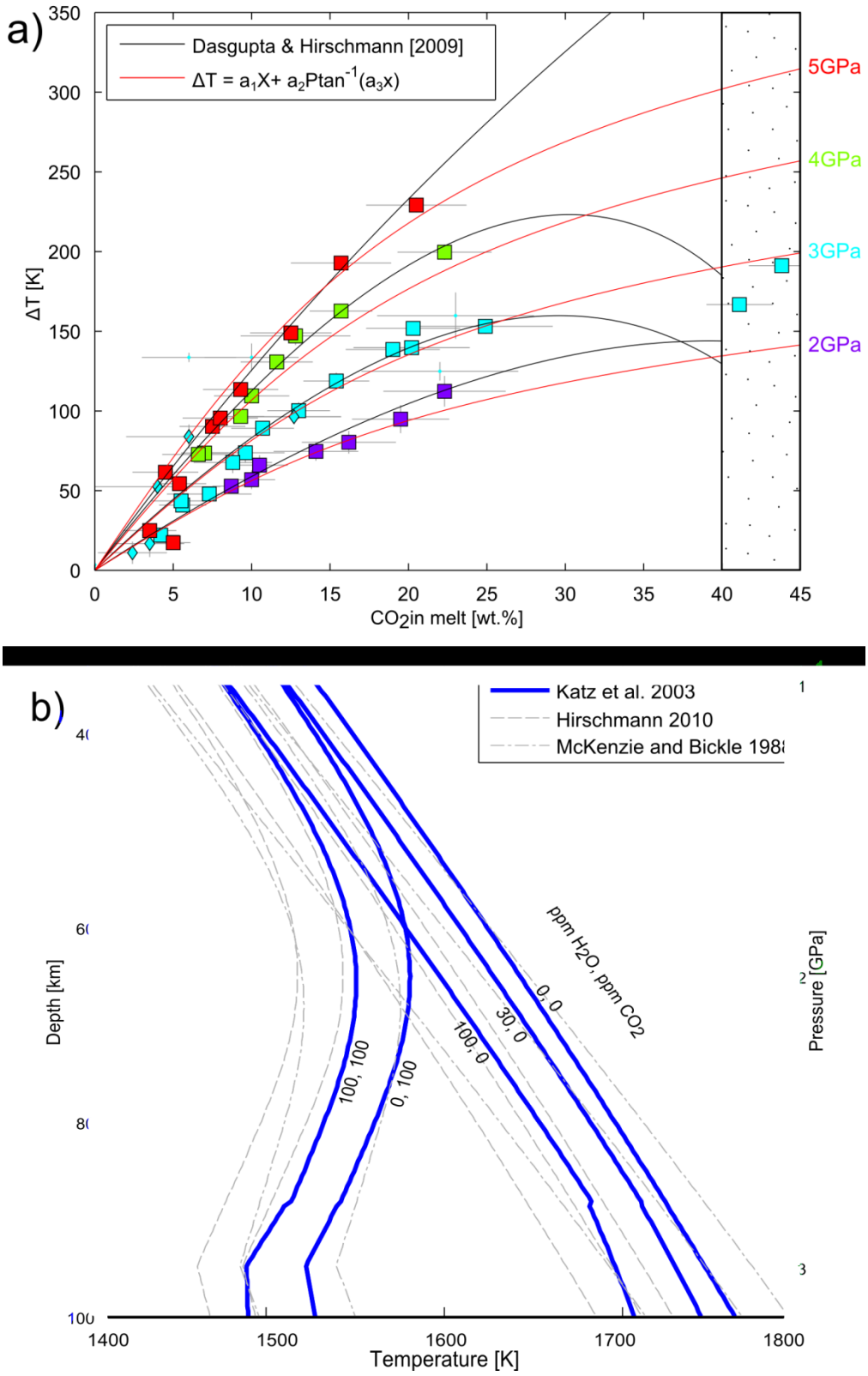

Figure 3:a) Model of peridotite solidus depression as a function of CO_2 in melt and pressure, shown in red. Original model of Dasgupta et al. (2013) is shown for comparison. b) Plot of Katz et al. (2003) melting solidus as a function of pressure and depth for varying bulk H2O, CO_2 compositions. Models of Hirschmann (2010) and McKenzie and Bickle (1988) are shown in grey for comparison.

Carbonated-silicate melt conductivity model

The experimental results of Yoshino et al. (2012a) on carbonated melt with variable CO_2 concentration was fit by the form:

$$\log \sigma_m = (b_1 X + b_2) - \left(\frac{150 - 56\frac{X}{25})}{RT * \log(10)} \right)$$

Where b_1= -5.36e-2 , b_2=5.56 (Figure 4).For comparison, silicate and carbonatite samples, taken from Pommier et al. (2010), Yoshino et al. (2012a), and Gaillard et al. (2008) are included.

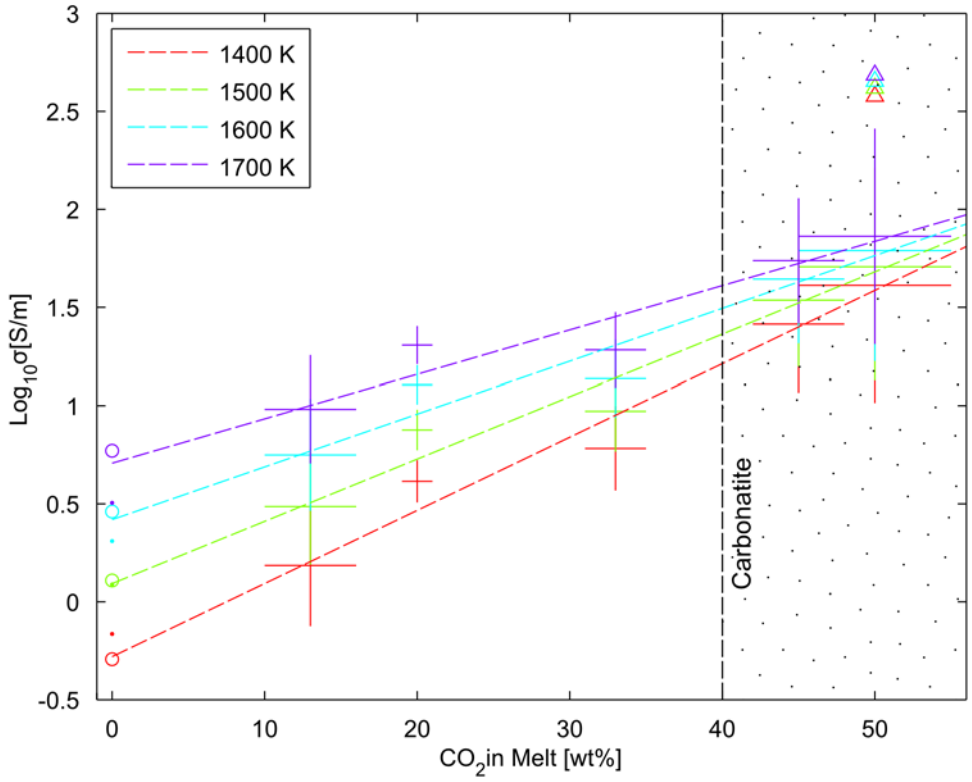

Figure 4:Conductivity model of data of Yoshino et al. (2012a) for carbonated silicate melt as a function of temperature and CO_2 concentration in melt. Original data of Yoshino et al. (2012a) is plot as crosses. For comparison, melt conductivity data of Pommier et al. (2010), Yoshino et al. (2010), and Gaillard et al. (2008) have been plot as circles, points, and stars respectively, by the Arrhenius relationship.

Bulk Conductivity model

The conductivity effects of a carbonated silicate melt as an immiscible melt phase were combined in HS bounds with the conductivity of silicate and olivine phases taken from Pommier et al. (2010) and Poe et al. (2010), Yoshino et al. (2009) respectively.

The comparison of the upper and lower HS bounds for each of the melt models as a function of bulk water content show a dependence on the melt model used (Figure 5)

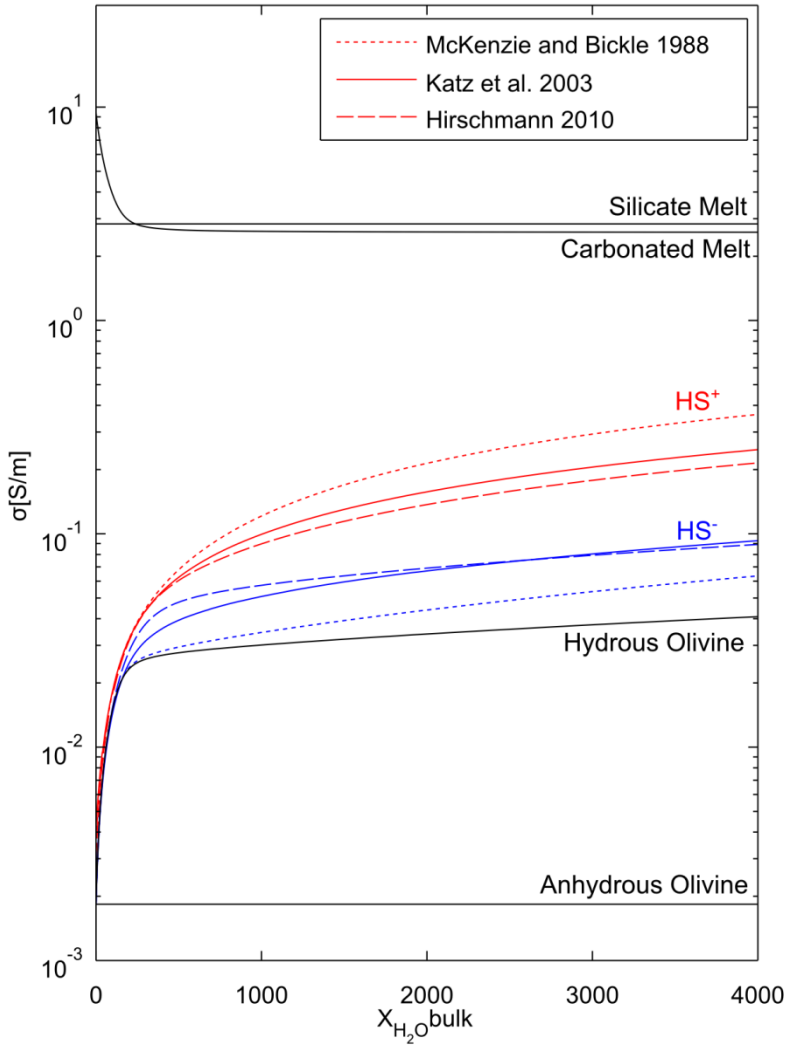

Figure 5:Conductivity Hashin-Shtrikman bounds for the three melting functions at isobaric pressure, as a function of bulk water content. Conductivityes of Hydrous olivine, hydrated carbonated melt, silicate melt from Pommier et al. (2010), and anhydrous olivine are plot for comparison

DISCUSSION

Discussion of Models Presented

SOLIDUS DEPRESSION MODEL

Our model of solidus depression as a function of CO_2 and pressure is a significant improvement on the original fit by Dasgupta et al. (2013). Their study did not present a model that could be applied outside their range of interest of CO_2 <25% and 2-5 GPa. However it can be seen that our model did not fit the ranges of 15-25 wt.% CO_2 at pressure 4 and 5 GPa as well as Dasgupta's (2013) model. This is due largely to the lack of available data in this region and Dasgupta et al. (2013)fitting each pressure individually. It may also be the case that Dasgupta (2013) did not use a weighted fitting method for their data which allowed for a more direct fit. Regardless of this, it can be seen that our model fit is still well within the error bounds of valid data points. Although the model is a close fit to the 3GPa data at 40-50 wt.% CO_2, the lack of available data beyond 25 wt.% CO_2 and other pressures is a substantial restriction of this model. In the availability of a more extensive dataset it would be worthwhile to revisit this model.

Figure 6 shows the comparison of variations of bulk CO_2 in each melting models. As expected, the reduction in solidus temperature is very significant, with up to 200 degree reduction for eve shallow depths. Consequently, melting is much more significant at great depths, in comparison to models that do not include bulk CO_2.

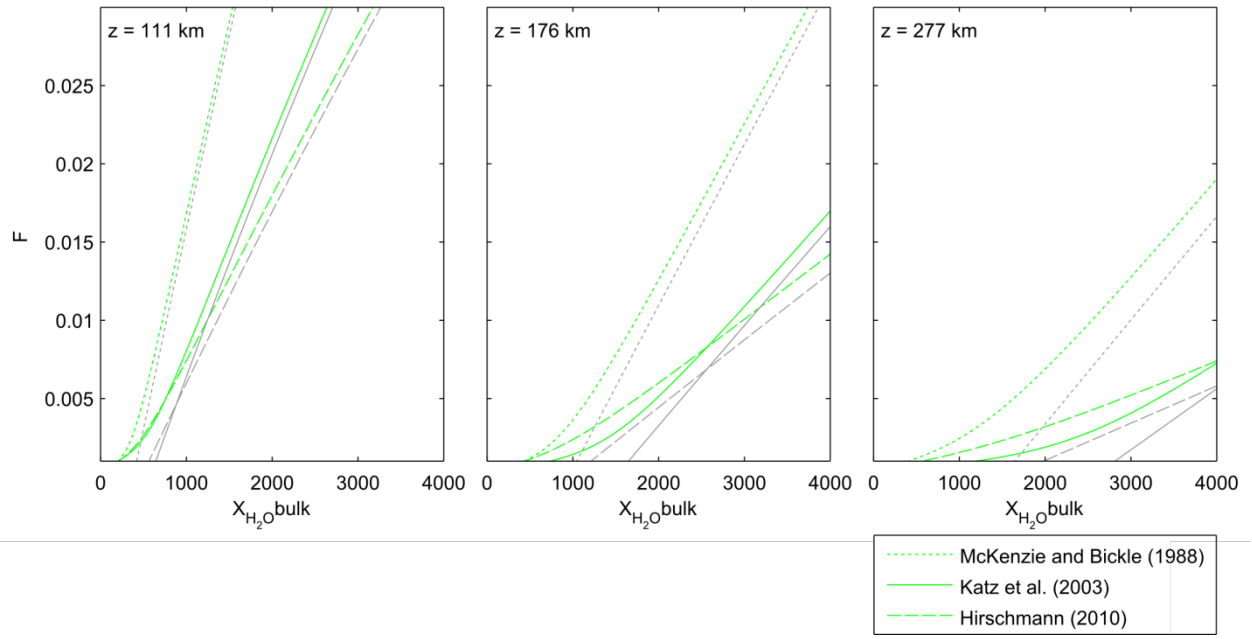

Figure 6:Comparison of models of melt fraction at depth with the effect of 100ppm bulk CO_2 (green plot) and without (grey plots).

It can be seen that while McKenzie and Bickle (1988) model has a good agreement of melt fraction for great depths, it suffers from significant overestimation of melt fraction as a function of bulk water content at shallow depths in comparison (12% difference for 0.1% bulk water). For low bulk water content the models ofHirschmann (2010) and Katz et al. (2003) are in very close agreement (<<1% F difference for bulk H2O < 1000ppm), however the separation of the two increases with increasing pressure and solubility of melt (>3% difference for bulk H2O >4000ppm). This is largely due to the model Katz et al. (2003) accounting for the increase in melt production from clinopyroxene melting.

CARBONATED-SILICATE MELT CONDUCTIVITY MODEL

Linearly fitting the pre exponential factors of 5 samples proved to be in good agreement at the intercept (5.56 log units) with the results for silicate melts of Tyburczy and Waff (1983) (4.5-6 log units) and Pommier et al. (2010)(6.08 log units). For carbonitic

composition, the values for dolomite used in the study of Yoshino et al. (2012a)(1343 S/m), are slightly lower than the mantle carbonatite values reported by (Gaillard et al. 2008) (3440 S/m).

The linear model in Figure 4 is of great agreement at the intercept with the Arrhenius relationship values of Pommier et al. (2010)for Kilauea basalt, which is the basaltic melt phase conductivity used in this study. Note however in Figure 4Figure 5, where CO_2 concentration in carbonated melt is washed out by increasing silicate melting as bulk hydration increases. Here the conductivity of carbonate melts is slightly lower than that of the Kilauea basaltic melt. Although we expected the carbonated melt conductivity to asymptote from above to that of anhydrous silicate melt, we see this difference of 0.2 log units to have insignificant effect on bulk conductivity.

However the model shown Figure 4 is in very poor agreement with the mantle Cabonitites of Gaillard et al. (2008). Yoshino et al. (2012a) addressed this discrepancy, commenting that the values reported by Gillard are alkali carbonate melts, which have a slightly higher conductivity than alkali free carbonate melts. The effects of alkalis on the conductivity of melts has been of interest of a number of papers (e.g. Pommier and Garnero (2014)), and parameterising the effects of alkalis on carbonated and silicate melt conductivities would be beneficial for future studies.

MANTLE MODEL

The mantle conductivity model produced in this study makes 4 assumptions:

- The mantle is adiabatically upwelling.
- The mantle is a 3 phase system of olivine, carbonated silicate melts, and silicate melts.
- Carbonated-silicate melts and silicate melts are immiscible phases.

- Melt hydration does not affect the melt conductivity.
- The maximum hydration of the solid phase, Is given by the saturation of olivine
- The mantle is metastable (i.e. the mantle is not currently undergoing change with time)

This is a very generalised, and simple view of mantle, and we acknowledge that while it is a good basis for interpretations, our model is not globally assured, namely in systems that are rapidly evolving. We also believe that the limiting hydration of the solid phase at olivine saturation is an incorrect assumption as the saturation point of the pyroxenes are as much as 6-12 times that of olivine (Wang et al. 2008, O'Leary et al. 2010). However we did not consider this in our models there is little knowledge of how this saturation point and the partitioning of water behaves as a function of great depths. In future studies it would be of benefit to incorporate effects of different mineralogies, alkali composition, and hydration of the carbonate-silicate melt and silicate melt.

The reader is directed to observe Figure 5, which shows the behaviour of conductivity bounds as a function of bulk water content at a chosen depth, for multiple melting models. It is important to here to reiterate that the either HS bound does not indicate the true conductivity value, but an absolute bound in absence of knowledge of the geometrical arrangement of the phases. In common practice however it is seen that experimental data more closely follows the upper bound (e.g. (Yoshino et al. 2010, Pommier and Garnero 2014, Ni et al. 2011)). Therefore, we similarly expect the true

conductivity of the system to be more closely bound to the upper Hashin-Shtrikman bound.

GEOPHYSICAL IMPLICATIONS

For the remainder of this study, we compare the application of our model to conductivity data of (Key et al. 2013) for the East Pacific Rise, and(Wannamaker et al. 2008) for the central great basin, with other previous interpretations of the area.

EPR

The magnetotelluric experiment of (Key et al. 2013) observes conductivity as high as 3.33 S/m beneath the EPR at 50 km depth. However, at this depth and at under adiabatic temperatures, this conductivity range is not possible under our model, as the largest concentration of CO_2 in carbonated melt achievable at this depth was 1.8 wt.%, corresponding to a carbonated melt conductivity of only 2.7 S/m [which is the most conductive phase]. Key et al. (2013) acknowledges that it may be that the highly abnormal conductivity range could be the result of the inversion trading-off the narrow size for the anomaly with a compensating higher conductivity.

Excluding this above outlier, Key et al. (2013) reports the conductivity of the main conductive body between 30 and 70km deep to have resistivities of 1-10 ohm/m, a range our model finds possible with <20% melt for 1-3 ohm/m and <5% for 8-10 ohm/m. The 10–60ohm/m resistivity below this at 100km we report being possible with 0-2% melt, and 0-0.1% bulk water.

These melt fraction ranges are within acceptable range of values claimed by Key et al. (2013), however the high 1 ohm/m interpretations of <20% melt, disagree significantly with seismic interpretations of <3% (Toomey et al. 1998, Hammond and Toomey

2003). If these values are not also due to inversion error, it is likely that conductivity is dominated by chemical effects not included in our study, for example the effect of alkalis such as sodium, which is observed to cause resistivities as low as 0.05 ohm/m for very small melt fraction (Pommier et al. 2013).

BASIN AND RANGE

Using the conductivity-depth profile of Wannamaker et al. (2008) (Figure 7) the range of melt fraction and hydration achievable is plotted for each of the 3 melt fraction models (Figure 8)

Decoupling of EM fields into orthogonal components (Transverse Electric and Transverse Magnetic polarisation) is useful to observe the upper and lower bounds of conductivity due to electrical anisotropy of the mantle (Thiel 2008). The BR conductivity data of Wannamaker et al. (2008) has been measured TM and TE modes in the N-S and E-W directions respectively, and observes lower resistivity in the N-S direction than in the E-W, by as much as 1.2 ohm/m difference. It is therefore appropriate to model the more resistive N-S direction by the lower HS bounds, representative of isolated conductive phase in a resistive matrix, and the more conductive E-W direction by the upper HS bounds, which represents a resistive phase in a conductive matrix.

Applying our mantle conductivity model to the basin and range data is interpreted by observing the overlap of the HS bounds of the resistive NS direction with those in the conductive EW direction . 100ppm bulk CO_2 has is chosen as an upper limit, as the mantle typically contains <= 100ppm CO_2 (Dasgupta et al. 2013).

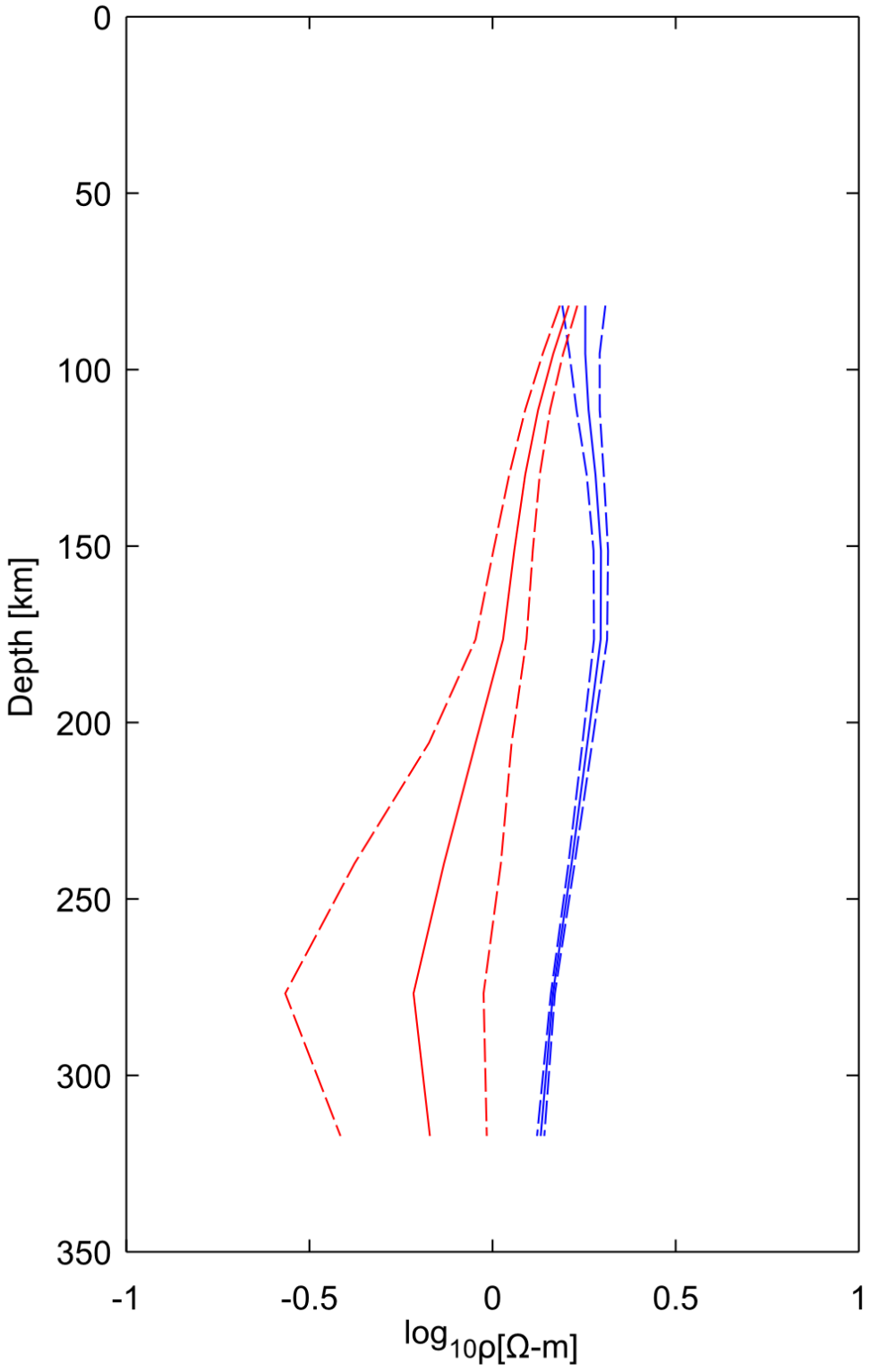

Figure 7:Conductivity depth profile taken form Wannamaker et al. (2008). Red and blue are assigned to E-W and N-S measurements. Dashed line represents upper and lower bound of conductivity range at that depth

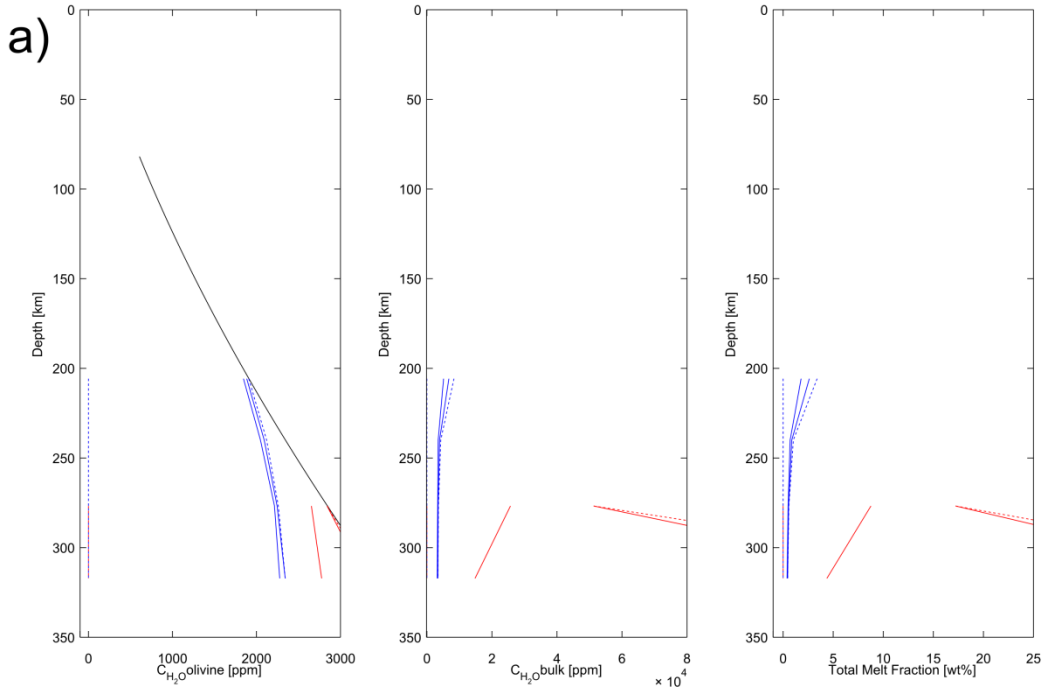
a)
Depth [km]
0
50
100
150
200
250
300
350
0
1000
2000
3000
C_{H_2O}olivine [ppm]
0
2
4
6
8
C_{H_2O}bulk [ppm]
× 10^4
0
5
10
15
20
25
Total Melt Fraction [wt%]

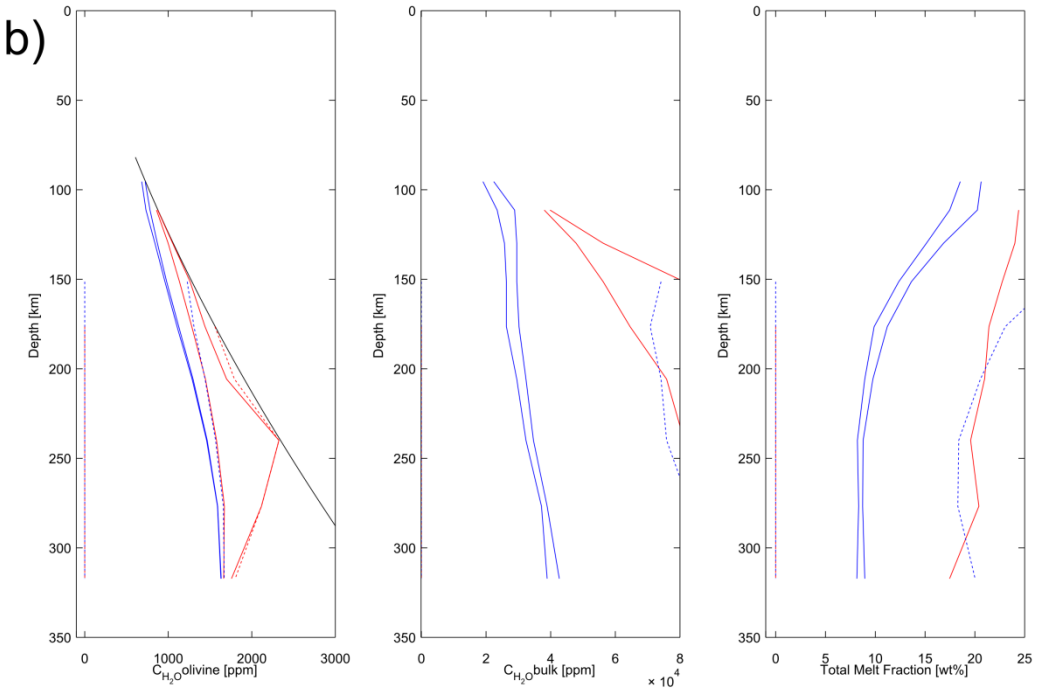
b)
Depth [km]
0
50
100
150
200
250
300
350
0
1000
2000
3000
C_{H_2O}olivine [ppm]
0
2
4
6
8
C_{H_2O}bulk [ppm]
× 10^4
0
5
10
15
20
25
Total Melt Fraction [wt%]

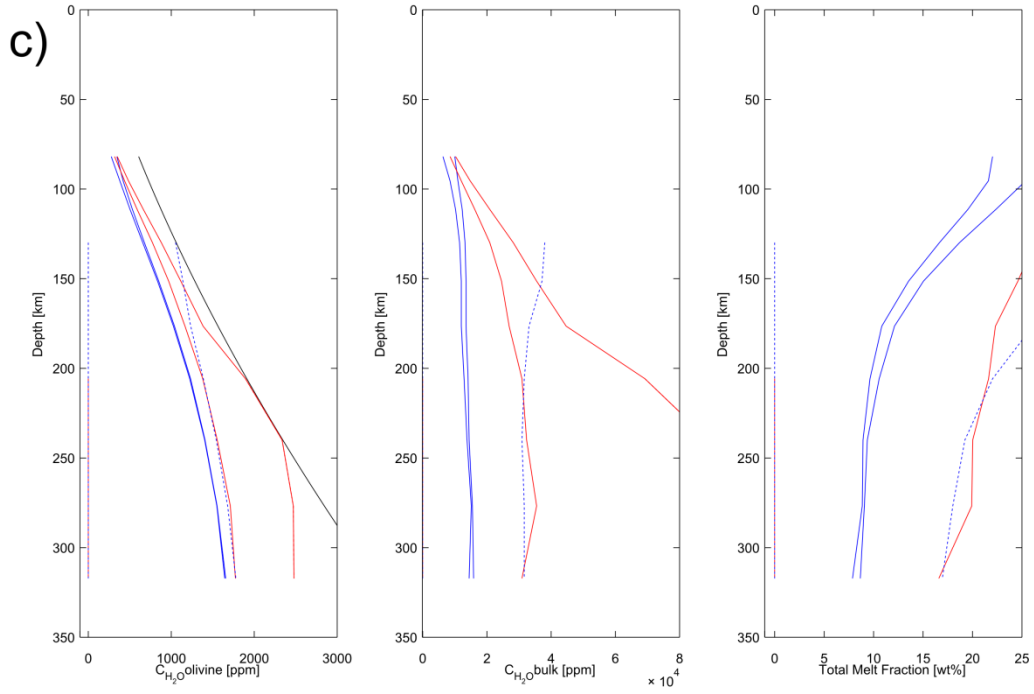

Figure 8:Manlte properties Olivine hydration (black line indicates saturation), bulk water content, and melt fraction, as a function of depth plot using melting method: a)Katz et al. 2003, b)Hirschmann 2010, c)McKenzie and Bickle 1988. Dashed line represents range calculated with the upper lower HS bound on conductivity, solid line represents range calculated with the upper HS bound on conductivity. Red and blue are assigned to E-W and N-S measurements.

However, due to the nature of Kat's melting model requiring far more water to initiate melting (Figure 6), the saturation of olivine was approached far more rapidly in this model, which results in undetermined bounds. as we acknowledge there is significantly higher water saturation of pyroxene and is a likely solution to this problem for future studies

Without over interpreting the figures, there is a general agreement of that the melt fraction exist as ~10% at depths between 175 to 300 km, and as much >25% as we approach the moho. The melting model of McKenzie and Bickle (1988) places an upper limit o bulk water content at 4%, however we believe it is more likely for the bulk

water content of the mantle to be found in the range of 2-3%, which is a an acceptable range.

We believe that this significant increase of melt fraction as we approach the Moho, is indicative of magmas pooling at the base of the crust, which is in support of the theory posed by Wannamaker et al. (2008), that extension in the Great Basin-Colorado Plateau, is by mode of simple shear along detachment faults.

CONCLUSIONS

In this study we have parameterised the effect that carbonated melts have on melting and conductivity, following on from work of (Dasgupta et al. 2013) and Yoshino et al. (2012b). By then incorporating these effects, we have created a model that predicts variations in melt fraction and bulk hydration in an adiabatic mantle, with the presence of carbonated silicate melts, that agrees very well with case studied in the East Pacific Rise, and the Central Great Basin.

ACKNOWLEDGMENTS

I would like to thank my Honours Geophysics peers, Derrick Hasterok, and Lily Upton for their academic assistance and support throughout the year.

REFERENCES

CARCIONE J. M., URSIN B. & NORDSKAG J. I. 2007 Cross-property relations between electrical conductivity and the seismic velocity of rocks, *Geophysics,* vol. 72, no. 5, pp. E193-E204.

CONSTABLE S. 2006 SEO3: A new model of olivine electrical conductivity, *Geophysical Journal International,* vol. 166, no. 1, pp. 435-437.

CONSTABLE S. & HEINSON G. 2004 Hawaiian hot-spot swell structure from seafloor MT sounding, *Tectonophysics,* vol. 389, no. 1–2, pp. 111-124.

DAI L. & KARATO S.-I. 2009 Electrical conductivity of orthopyroxene: Implications for the water content of the asthenosphere, *Proceedings of the Japan Academy, Series B,* vol. 85, no. 10, pp. 466-475.

DASGUPTA R. & HIRSCHMANN M. M. 2006 Melting in the Earth's deep upper mantle caused by carbon dioxide, *Nature,* vol. 440, no. 7084, pp. 659-662.

--- 2010 The deep carbon cycle and melting in Earth's interior, *Earth and Planetary Science Letters,* vol. 298, no. 1–2, pp. 1-13.

DASGUPTA R., HIRSCHMANN M. M. & SMITH N. D. 2007a Partial Melting Experiments of Peridotite + CO2 at 3 GPa and Genesis of Alkalic Ocean Island Basalts, *Journal of Petrology,* vol. 48, no. 11, pp. 2093-2124.

DASGUPTA R., HIRSCHMANN M. M. & SMITH N. D. 2007b Water follows carbon: CO2 incites deep silicate melting and dehydration beneath mid-ocean ridges, *Geology,* vol. 35, no. 2, pp. 135-138.

DASGUPTA R.*, et al.* 2013 Carbon-dioxide-rich silicate melt in the Earth's upper mantle, *Nature,* vol. 493, no. 7431, pp. 211-215.

DAVIES J. H. & BICKLE M. J. 1991 A Physical Model for the Volume and Composition of Melt Produced by Hydrous Fluxing above Subduction Zones, *Philosophical Transactions of the Royal Society of London. Series A: Physical and Engineering Sciences,* vol. 335, no. 1638, pp. 355-364.

DVORAK Z. 1973 Electrical conductivity of several samples of olivinites, peridotites, and dunites, as a function of pressure and temperature, *Geophysics,* vol. 38, no. 1, pp. 14-24.

GAILLARD F. 2004 Laboratory measurements of electrical conductivity of hydrous and dry silicic melts under pressure, *Earth and Planetary Science Letters,* vol. 218, no. 1–2, pp. 215-228.

GAILLARD F.*, et al.* 2008 Carbonatite Melts and Electrical Conductivity in the Asthenosphere, *Science,* vol. 322, no. 5906, pp. 1363-1365.

GREEN D. H. & RINGWOOD A. E. 1963 Mineral assemblages in a model mantle composition, *Journal of Geophysical Research,* vol. 68, no. 3, pp. 937-945.

HAMMOND W. C. & TOOMEY D. R. 2003 Seismic velocity anisotropy and heterogeneity beneath the Mantle Electromagnetic and Tomography Experiment (MELT) region of the East Pacific Rise from analysis of P and S body waves, *Journal of Geophysical Research: Solid Earth,* vol. 108, no. B4, p. 2176.

HASHIN Z. & SHTRIKMAN S. 1963 A variational approach to the theory of the elastic behaviour of multiphase materials, *Journal of the Mechanics and Physics of Solids,* vol. 11, no. 2, pp. 127-140.

HASTEROK D. 2014 Mixing Model. In KEANE A. ed.

HIROSE K. 1997 Partial melt compositions of carbonated peridotite at 3 GPa and role of CO2 in alkali-basalt magma generation, *Geophysical Research Letters,* vol. 24, no. 22, pp. 2837-2840.

HIRSCHMANN M. M. 2000 Mantle solidus: Experimental constraints and the effects of peridotite composition, *Geochemistry, Geophysics, Geosystems,* vol. 1, no. 10, p. 1042.

--- 2010 Partial melt in the oceanic low velocity zone, *Physics of the Earth and Planetary Interiors,* vol. 179, no. 1–2, pp. 60-71.

HIRSCHMANN M. M., AUBAUD C. & WITHERS A. C. 2005 Storage capacity of H2O in nominally anhydrous minerals in the upper mantle, *Earth and Planetary Science Letters,* vol. 236, no. 1–2, pp. 167-181.

KATZ R. F., SPIEGELMAN M. & LANGMUIR C. H. 2003 A new parameterization of hydrous mantle melting, *Geochemistry, Geophysics, Geosystems,* vol. 4, no. 9, p. 1073.

KELBERT A., SCHULTZ A. & EGBERT G. 2009 Global electromagnetic induction constraints on transition-zone water content variations, *Nature,* vol. 460, no. 7258, p. 4.

KEY K.*, et al.* 2013 Electrical image of passive mantle upwelling beneath the northern East Pacific Rise, *Nature,* vol. 495, no. 7442, pp. 499-502.

LEDO J. & JONES A. G. 2005 Upper mantle temperature determined from combining mineral composition, electrical conductivity laboratory studies and magnetotelluric field observations: Application to the intermontane belt, Northern Canadian Cordillera, *Earth and Planetary Science Letters,* vol. 236, no. 1–2, pp. 258-268.

MCKENZIE D. & BICKLE M. J. 1988 The Volume and Composition of Melt Generated by Extension of the Lithosphere, *Journal of Petrology,* vol. 29, no. 3, pp. 625-679.

NI H., KEPPLER H. & BEHRENS H. 2011 Electrical conductivity of hydrous basaltic melts: implications for partial melting in the upper mantle, *Contributions to Mineralogy and Petrology,* vol. 162, no. 3, pp. 637-650.

O'LEARY J. A., GAETANI G. A. & HAURI E. H. 2010 The effect of tetrahedral Al3+ on the partitioning of water between clinopyroxene and silicate melt, *Earth and Planetary Science Letters,* vol. 297, no. 1–2, pp. 111-120.

POE B. T.*, et al.* 2010 Electrical conductivity anisotropy of dry and hydrous olivine at 8GPa, *Physics of the Earth and Planetary Interiors,* vol. 181, no. 3, pp. 103-111.

POMMIER A. 2012 Sigmelts. School of Earth and Space Exploration: Arizona State University.

POMMIER A.*, et al.* 2010 Methodological re-evaluation of the electrical conductivity of silicate melts, *American Mineralogist,* vol. 95, no. 2-3, pp. 284-291.

POMMIER A. & GARNERO E. 2014 Petrology-based modeling of mantle melt electrical conductivity and joint interpretation of electromagnetic and seismic results, *Journal of Geophysical Research: Solid Earth*.

ROBERTS J. J. & TYBURCZY J. A. 1999 Partial-melt electrical conductivity: Influence of melt composition, *Journal of Geophysical Research: Solid Earth,* vol. 104, no. B4, pp. 7055-7065.

SELVERSTONE J., PUN A. & CONDIE K. C. 1999 Xenolithic evidence for Proterozoic crustal evolution beneath the Colorado Plateau, *Geological Society of America Bulletin,* vol. 111, no. 4, pp. 590-606.

SIMPSON F. 2002 Intensity and direction of lattice-preferred orientation of olivine: are electrical and seismic anisotropies of the Australian mantle reconcilable?, *Earth and Planetary Science Letters,* vol. 203, no. 1, pp. 535-547.

SIMPSON F. & BAHR K. 2005 Practical magnetotellurics*.* Cambridge University Press.

THIEL S. 2008 Modelling and inversion of magnetotelluric data for 2-D and 3-D lithospheric structure, with application to obducted and subducted terranes. School of Earth and Environmental Sciences : Geology and Geophysics*.* University of Adelaide.

TOOMEY D. R.*, et al.* 1998 Mantle Seismic Structure Beneath the MELT Region of the East Pacific Rise from P and S Wave Tomography, *Science,* vol. 280, no. 5367, pp. 1224-1227.

TYBURCZY J. A. & WAFF H. S. 1983 Electrical conductivity of molten basalt and andesite to 25 kilobars pressure: Geophysical significance and implications for charge transport and melt structure, *Journal of Geophysical Research: Solid Earth,* vol. 88, no. B3, pp. 2413-2430.

WANG D.*, et al.* 2008 The electrical conductivity of upper-mantle rocks: water content in the upper mantle, *Physics and Chemistry of Minerals,* vol. 35, no. 3, pp. 157-162.

WANNAMAKER P. E.*, et al.* 2008 Lithospheric dismemberment and magmatic processes of the Great Basin–Colorado Plateau transition, Utah, implied from magnetotellurics, *Geochemistry, Geophysics, Geosystems,* vol. 9, no. 5.

WNNORENDT R. F. & MYSPX B. O. 1980 Melting phase relations of natural peridotite+ CO2 as a function of degree of partial melting at 15 and 30 kbar, *American Mineralogist,* vol. 65, pp. 37-44.

XU Y., SHANKLAND T. J. & POE B. T. 2000 Laboratory-based electrical conductivity in the Earth's mantle, *Journal of Geophysical Research: Solid Earth,* vol. 105, no. B12, pp. 27865-27875.

YANG X.*, et al.* 2011 Effect of water on the electrical conductivity of lower crustal clinopyroxene, *Journal of Geophysical Research: Solid Earth,* vol. 116, no. B4, p. B04208.

YOSHINO T.*, et al.* 2010 Electrical conductivity of basaltic and carbonatite melt-bearing peridotites at high pressures: Implications for melt distribution and melt fraction in the upper mantle, *Earth and Planetary Science Letters,* vol. 295, no. 3–4, pp. 593-602.

YOSHINO T.*, et al.* 2009 The effect of water on the electrical conductivity of olivine aggregates and its implications for the electrical structure of the upper mantle, *Earth and Planetary Science Letters,* vol. 288, no. 1–2, pp. 291-300.

YOSHINO T.*, et al.* 2012a Electrical conductivity of partial molten carbonate peridotite, *Physics of the Earth and Planetary Interiors,* vol. 194–195, no. 0, pp. 1-9.

YOSHINO T.*, et al.* 2012b Effect of temperature, pressure and iron content on the electrical conductivity of olivine and its high-pressure polymorphs, *Journal of Geophysical Research: Solid Earth,* vol. 117, no. B8, p. B08205.

APPENDIX A: YOSHINO ET AL. 2012 MODEL FUNCTIONS

ASSUMPTIONS OF THE DATA

- Best fits appear to be simple second order polynomials
- The points converge as X increases (i.e. T has a diminishing effect on conductivity, as X increases)
- Why? Can we make a relation about this from the prexisting data?
- Ideally, the points should not converge before X=100, and even then the curves shouldn't intersect. However, having a model that only is valid up to X=60 is still acceptable, as it is unlikely that we will find X>45 (dolomite/carbonatite?)
- The slope of the fit should *never* be negative for X>0
- The separation of the points is a linear function of X
- if you plot X vs (cond(1700K,X) - cond(1400K,X)), for all points X, you get a perfectly straight line between the points.
- this also works for any other two temps, with near non existant residuals!
- Evidently, this is due to the functions these points were plotted with, but I cant work it out. The original functions may be functions of T leading to a consistent temperature difference for one point (one X value) but each point should be independent?
- This has to be something to do with how dH and Logs0 were created, and therefore our equation should take this into account, not use some constant
- Therefore, as and Logs0 were not measured, but estimated over a linear range between silicate, and dolomite melts, can we really use his data to create a model?

EMPIRICAL FUNCTION

This is the function I created earlier.

Initially the conductivity data was fitted for each temperature as a function of X:

$$Log\sigma(X) = a_1X^2 + a_2X + a_3$$

However this did not incorporate T into the function

as separation of fits was a linear function of X, inverse linearly related to the closeness to X=Xconv, (ie at X=Xconv, DT=0, at X=0, DT is a mximum)

I was able to make the below relationship:

$$\Delta Log\sigma(X, T_1, T_2) = \left(Log\sigma(X = 0, T_2) - Log\sigma(X = 0, T_1)\right) \times (1 - \left(\frac{X}{X_{conv}}\right))$$

Which is the separation of the 2 polynomials at T1 and T2. this will return max separation at X=0, and no separation at X=conv.

As we are only interested in one unknown temp, we can use a known temp T0 (1400K) with a known Logs(0,t0) value (i.e. known y intercept, labelled C):

$$\Delta Log\sigma(X, T) = (Log\sigma(X_0, T) - C) \times (1 - \left(\frac{X}{X_{conv}}\right))$$

As we already know the Logs function for 1400K, *and* the separation between the T0=1400K fit and any fit for any given X and T, we can then imply the conductivity for any given X and T

$$Log\sigma(X, T) = Log\sigma(X, T_0) + \Delta Log\sigma(X, T)$$

$$Log\sigma(X, T) = Log\sigma(X, T_0) + (Log\sigma(X_0, T) - C) \times (1 - \left(\frac{X}{X_{conv}}\right))$$

Now we have the conductivity difference between the lowest temp (which in the figure is 1400K) and a temp of interest T, for a given X. However we don't know what

logs(X0,T) is

By plotting the intercept of 30 different temperatures, it can be seen that there is a polynomial trend of the intercepts (see subplots) as a function of temperature, and we can extrapolate this to logs(X0,T) (a function of Temperature):

$$Log\sigma(X_0, T) = b_1T^2 + b_2T + b_3$$

$$Log\sigma(X, T) = Log\sigma(X, T_0) + (a_1T^2 + a_2T + a_3 - C) \times (1 - \left(\frac{X}{X_{conv}}\right))$$

And as mentioned, we know Logs(X,T0) from fitting the data of 1400 K:

$$Log\sigma(X, T) = (a_1X^2 + a_2X + a_3) + (b_1T^2 + b_2T + b_3 - C) \times (1 - \left(\frac{X}{X_{conv}}\right))$$

and recall that C is Logs(X,T0) at X=0:

$$Log\sigma(X, T) = (a_1X^2 + a_2X + C) + (b_1T^2 + b_2T + b_3 - C) \times (1 - \left(\frac{X}{X_{conv}}\right))$$

However the problem with this fit is that the initial polynomial fits are a piece of shit at higher temps and low x, mainly because assumption3 is not met.
What we want for a better fit is to get rid of a_2, but still maintain X_conv, a point which is prevalent even in the point difference plot

Separation of polynomial

$$Log\sigma\left(T, X_{CO_2}\right) = (a_1T^2 + a_2T + a_3 - b_3)\left(1 - \left(\frac{X}{X_{conv}}\right)\right) + (b_1X^2 + b_2X + b_3)$$

FUNCTION 1

This is the simplest option, where it is the polynomial fit, but b=0, such that when x=0, y'=0, satisfying assumption 3. To maintain xconv, we would expect a shallowing function as T increases.

to do this: $a \times b \equiv \frac{log\sigma}{X^2+1}$ but I have no idea how to do this

$\log \sigma_m = ax^2 + b \qquad f'(x) = 2ax$

$f'(a) = x^2 \qquad f'(b) = 1$

using this function actually returned surprisingly similar results. the only part of the empirical function that changes is part 1 to the form:

$Log\sigma(X) = a_1X^2 + a_3$

rms misfits are constant, so using the same method as prior should be fine, resulting in:

$Log\sigma(X,T) = (a_1X^2 + C) + (b_1T^2 + b_2T + b_3 - C) \times (1 - \left(\frac{X}{X_{conv}}\right))$

Where a,b,C, X_conv are all constants

HOWEVER. this has buggered us up, as the derrivative wrt x, is sometimes <0.

WHICH SHOULD NEVER HAPPEN. this is a fault with choosing a simple linear form of DLog, which was created BY FITTING A MODEL TO THE MODEL

However we are doing this evidently anyways, i need to look at the ypshino paper again

for more info about why the difference is so shitting linear.

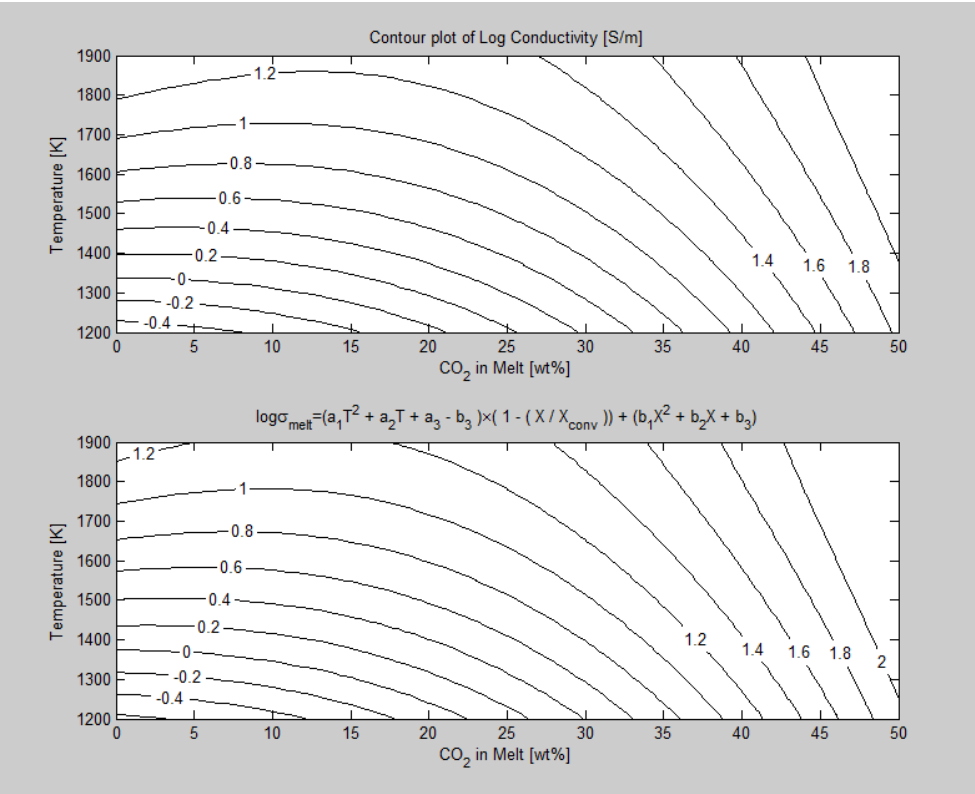

FUNCTION 2

Same as above, but by determining Xconv, and Logconv beforehand,

$$y = ax^2 + b$$

$$y_c = ax_c^2 + b$$

$$b = y_c - ax_c^2$$

$$y = ax^2 + (y_c - ax_c^2)$$

$$y = a(x^2 - x_c^2) + y_c$$

$$\log \sigma_m = a(X^2 - X_{conv}^2) + \log \sigma_m (X_{conv}) \quad y' = 2aX$$

$$\log \sigma_m (X = 0) = (-aX_{conv}^2) + \log \sigma_m (X_{conv})$$

a controls the shallowness of the function, while being anchored by X. the shallower function describes the higher temp. therefore, a will be a function of temp.

If we get the original function that took T into account when calculating conductivity for a given X, then we might be able to use the approprite relation. Key features of T dependance:

with increasing X, the effect on Logs lessens

could be implied by the vertical intercept of an ax^2+b fit

eg $(-aX_{conv}^2) + \log \sigma_m\,(X_{conv}) =$ some vertical intercept, and then go form there

we need to make sure that the derrivative of logs>=0

there are only 2 things that contol this function:

the anchor point (xconv); and

a.

you cant fuck this up.

if a controls the vertical intercept, then it is likely a 2nd order polynomial, as decribed in points 6 & 7

Input interpretation:

$$\text{plot}\ \left\{2.2 + \frac{-3600 + x^2}{1000},\ 2.2 + \frac{-3600 + x^2}{10\,000}\right\}\ x = 0 \text{ to } 61$$

Plot:

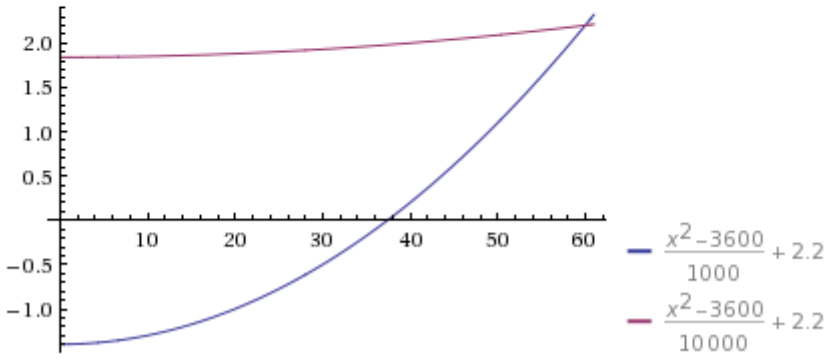

a smaller a gives a shallower function, therefore a must be inversely related to T

eg a=1/T

could try to relate the vertical intercepts

try and pull the T dependance from the original function!

Original function to plot points

$$\log \sigma_m = \log \sigma_0 - \left(\frac{dH}{RT}\right) \log(e^1)$$

R=8.314*10-3, which is consistent with a values tested, but we dont know dH at X=0

this equation implies at T~inf, we logσ approaches logσ0

however:

logσ0, and dH are functions of X.

these were calculated by having the greatest X sample to have logσ0, and dH of dolomite due to the high similarity in CO2 concentration, and no X to have logσ0, and dH of silicate basalt

dH was then assumed to vary linearly as a function of X between basaltic and carbonitic composition:

$$dH = dH_{dol} + (dH_{bas} - dH_{dol}) * \left(1 - \frac{X_{co2}}{50}\right)$$

so therefore we do know logσ0, and dH at X=0

logσ0 was also assumed to vary linearly as a function of X between basaltic and carbonitic composition; but it varied between Logs0 calculated for enthalpy of 150, and 38 kj/mol for each sample

eg the closeness of the sample composition to basaltic and carbonitic composition, weighted its logs0 values calculated for assumed 150 and 38kJ/mol enthalpies

$$Log\sigma 0_{38} = Log\sigma_{bulk} - \left(-\frac{38}{RT_{samp}}\right) * Log(e^1) + Log(C\varphi^n)$$

$$Log\sigma 0_{150} = Log\sigma_{bulk} - \left(-\frac{150}{RT_{samp}}\right) * Log(e^1) + Log(C\varphi^n)$$

$$Log\sigma 0 = Log\sigma 0_{38} + (Log\sigma 0_{150} - Log\sigma 0_{38}) * \left(1 - \frac{X_{co2}}{50}\right)$$

therefore the equation becomes:

$$\log \sigma_m = \log \sigma_0 - \left(\frac{dH_{dol} + (dH_{bas} - dH_{dol}) * \left(1 - \frac{X}{50}\right)}{RT}\right) \log_{10}(e^1)$$

$$\log \sigma_m = \log \sigma_0 - \left(\frac{38 + (112) * \left(1 - \frac{X}{50}\right)}{RT}\right) \log_{10}(e^1)$$

$$\log \sigma_m = \log \sigma_0 - \left(\frac{150 - 112(\frac{X}{50})}{RT}\right) \log_{10}(e^1)$$

$$\log \sigma_m = \log \sigma_0 - \left(\frac{150 - 56(\frac{X}{25})}{RT * \log(10)}\right)$$

but logσ0 is the unknown, as it stems from measurements

FUNCTION 3

. So we might have been going about it all wrong, we should have been **modelling logσ0** to put in the above equation(?)

but logσ0 as a function of what? (i guess X would be appropriate, seeing as it s logs0 measured for varying X values. can we extend the values to incorporate logs0 of dol and basalt? and dH of dol and basalt?

so this was done, it actually forms a relatively linear function:

$$\log \sigma_m = (\mathrm{aX} + \mathrm{b}) - \left(\frac{150 - 56(\frac{X}{25})}{RT * \log(10)} \right)$$

$$y'(x) = (a) + \left(\frac{56}{25RT * \log(10)} \right)$$

$$y'(T) = \frac{150 - \frac{56x}{25}}{RT^2 \log(10)}$$

$$y'(a) = (X)$$

$$y'(b) = (1)$$

we also need to determine the error of F and X effect on logs, but i have no idea how to calculate logs0. if i can do that i can substitute that in to the above equation, resulting a model built on data, not models. it should be:

$$Log\sigma 0_H = Log\sigma_{melt} - \left(-\frac{H}{RT_{samp}} \right) * Log(e^1)$$

$$Log\sigma 0_H = \left(Log\sigma_{bulk} - Log(C\varphi^n) \right) + \left(\frac{H}{RT_{samp}} \right) * Log(e^1)$$

but C and n seem to vary in some way in the samples. yoshino says "n has a value close to unity (1) for partially molten rocks" but in plotting this in fig 6, it is clear that they follow a different n value (~0.58) and different C values (the intercept (not log10))

as long as we get the same results, i dont hinbg the method is a problem

error in $Log\sigma 0_H$ is:

$$dLog\sigma 0_H = n \left(\frac{dF}{F * \log 10} \right)$$

note this has no dH dependence

therefore, error in $Log\sigma 0$ is:

$$dLog\sigma_0 = \sqrt{(dL\sigma_0)^2 + 2\left(\frac{dL\sigma_0 X}{50}\right)^2 + 2\left(\frac{L\sigma_0 dX}{50}\right)^2}$$

and the error in the second component of Logsm is:

$$-\frac{112dX}{50RT} * Log_{10}(e)$$

APPENDIX B: DASGUPTA 2013 FUNCTIONS

PLOTTING THE DATA/FUNCTION

Assumptions of the Data plot:

(see matlab script dDTdX.m)

1. The initial slope has a positive correlation to Pressure
2. At X~22, all slopes **appear** to converge to ~5
3. And therefore the slope decay is faster for higher pressures, and we would expect the double derivative to be a (linear?) function of pressure
4. This is something to consider, we can determine a,b,c, by setting x=22, and f'=5
5. The isobaric curves should **not** intersect, but may converge
6. At X=0, DT=0. Therefore there should be no additional constants
7. As the slopes of the isobaric curves appear to approach 0, we can assume that they asymptote out (which would be due to saturation of CO2 in the melt)

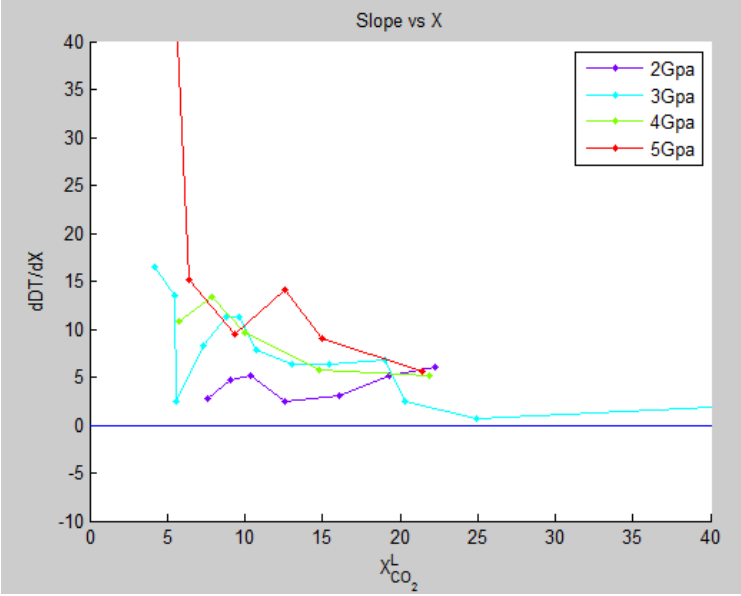

Possible functions:

FUNCTION 1

$f = ax + b \cdot \tan^{-1}(cx)$ $\quad (f'(x) = a + \frac{bc}{c^2x^2+1})$

$f'(a) = x \quad f'(b) = \tan^{-1}(cx) \quad f'(c) = \frac{bx}{c^2x^2+1}$

- a controls the slope of the asymptote, and creates a bi linear curve (should probably set a=0, or very close
- b is inversely proportional to the height of the asymptote
- c is proportional how rapidly the curve approaches asymptote

As a function of pressure:

$f = a \cdot x + bP \cdot \tan^{-1}(cx) \quad \left(f'(x) = a + \frac{bPc}{c^2x^2+1}\right) \quad (f'(P) = b \cdot \tan^{-1}(cx))$

$f'(a) = x \quad f'(b) = \tan^{-1}(cx) \quad f'(c) = \frac{bx}{c^2x^2+1}$

UNUSED FUNCTION

$f = a + b \cdot \ln(cx)$ $\quad (f'(x) = \frac{b}{x})$

$f'(a) = 1$ $\quad f'(b) = \ln(cx)$ $\quad f'(c) = \frac{b}{c}$

- a is proportional to the height of the function
- b is directly proportional to the slope (as a function of x)
- c is proportional to (also the height of the function?)
- root is at (x=exp(-a/b)/c)
- although this function does not pass through the origin, it can get very close by modifying the parameters. Otherwise, we could make a –ln component that is only significant at low X (this is actually what was done in Dasguptas supplementary equation)

FUNCTION 2

alternatively, to solve the origin problem

$f = a \cdot \ln(bx + 1)$ $\quad (f' = \frac{ab}{bx+1})$

$f'(a) = \ln(bx + 1)$ $\quad f'(b) = \frac{ax}{bx+1}$

as a function of pressure:

$f = aP \cdot \ln(bx + 1)$ $\quad (f'(x) = \frac{abP}{bx+1})$ $\quad f'(P) = a \cdot \ln(bx + 1)$

$f'(a) = P \cdot \ln(bx + 1)$ $\quad f'(b) = \frac{aP \cdot x}{bx+1}$

FUNCTION 3

$f = a - a\boldsymbol{e}^{-cx}$ $(f'(x) = ac\boldsymbol{e}^{-cx})$ $f'(P) = a - a\boldsymbol{e}^{-cx}$

$f'(a) = 1 - \boldsymbol{e}^{-cx}$ $f'(c) = ax\boldsymbol{e}^{-cx}$

a controls the asymptote location

b is proportional to the initial slope, and rate of approach to the asymptote

c is proportional to the initial slope and rate of approach to the asymatope

a == b for an origin pass-through, therefore c is a better control on the initial slope (?), and a==b is a control on the asymptote

both a==b and c would be a function of pressure (c may be better as a non-linear function of x)

As a function of pressure:

$f = aP - aP\boldsymbol{e}^{-cx}$ $(f'(x) = aPc\boldsymbol{e}^{-cx})$ $f'(P) = a - a\boldsymbol{e}^{-cx}$

$f'(a) = P - P\boldsymbol{e}^{-cx}$ $f'(c) = aPx\boldsymbol{e}^{-cx}$

FUNCTION 4

$f = \frac{ax}{b+cx^2}$ $(f' = \frac{a(b-cx^2)}{(b+cx^2)^2})$

$f'(a) = \frac{x}{b+cx^2}$ $f'(b) = -\frac{ax}{(b+cx^2)^2}$ $f'(c) = -\frac{ax^3}{(b+cx^2)^2}$

- a is proportional to the height of the peak, whilst still maintaining its location, by increasing the initial slope

- b is inversely propotional to the height of the peak, by changing its location by reducing the initial slope
- c is inversely proportional to the height of the peak, by changing its location whilst maintaining the initial slope.
- Unlike the other 3 functions, this one does not asymptote to a value (which would be the saturation point)
- $f' = 0$ at $x = \frac{\sqrt{b}}{\sqrt{c}}$ (we could make this the sat point, or add an additional logaritmic component that only becomes significant at this value)
- Sat point should be at about 45

FUNCTION 5

$f = aP\left(\frac{\boldsymbol{exp}(bx)-1}{\boldsymbol{exp}(bx)+1}\right)$ $f'(x) = 2abP\frac{\boldsymbol{exp}(bx)}{(\boldsymbol{exp}(bx)+1)^2}$ $(f'(P) =$

$a\left(\frac{\boldsymbol{exp}(bx)-1}{\boldsymbol{exp}(bx)+1}\right)$

$f'(a) = P\frac{\boldsymbol{exp}(bx)-1}{\boldsymbol{exp}(bx)+1}$ $f'(b) = 2aPx\frac{\boldsymbol{exp}(bx)}{(\boldsymbol{exp}(bx)+1)^2}$

a is proportional to the height of the asymptote

b is proportional to how rapidly the asymptote is approached

a would be

Plot: